Phytotoxins produced by *Phoma chenopodiicola*, a fungal pathogen of *Chenopodium album*

Marco Evidente,[a] Alessio Cimmino,[a] Maria Chiara Zonno,[b] Marco Masi,[a] Alexander Berestetskiy,[c] Ernesto Santoro,[d] Stefano Superchi,[d] Maurizio Vurro,[b] Antonio Evidente[a,*]

[a]Department of Chemical Sciences, University of Naples "Federico II", Complesso Universitario Monte S. Angelo, Via Cintia 4, 80126 Napoli, Italy

[b]Institute of Sciences of Food Production, National Research Council, Via Amendola 122/O, 70125 Bari, Italy

[c]All-Russian Institute of Plant Protection, Russian Academy of Agricultural Sciences, Pushkin, Saint-Petersburg 196608, Russia

[d]Department of Sciences, University of Basilicata, Via dell'Ateneo Lucano 10, 85100, Potenza, Italy

[*]Corresponding author. Tel.: +39 081 2539178; fax: +39 081674330
E-mail (address): evidente@unina.it (A. Evidente).

Abstract

Three phytotoxins were isolated from the liquid culture of *Phoma chenopodiicola*, a fungal pathogen proposed for the biological control of *Chenopodium album*, a common worldwide weed of arable crops. The three phytotoxins appeared to be a new tetrasubstituted furopyran, a new tetrasubstituted isocoumarin and a new *ent*-pimaradiene. They were characterized by using spectroscopic (essentially 1D and 2D NMR and HR ESI MS) and chemical methods as 3-(3-methoxy-2,6-dimethyl-7a*H*-furo[2,3-*b*]pyran-4-yl)-but-2-en-1-ol, 4,5,7-trihydroxy-3-methyl-isochroman-1-one, (1*S*,2*S*,3*S*,4*S*,5*S*,9*R*,10*S*,12*S*,13*S*)- 1,3,12-triacetoxy-2,hydroxy-6-oxo-*ent*-pimara-7(8),15-dien-18-oic acid 2,18-lactone, and consequently named chenopodolan D, chenisocoumarin and chenopodolin B. The absolute configuration to chenisocoumarin was assigned applying an advanced Mosher's method through the derivatization of it secondary hydroxylated carbon C-4, while that of chenopodolan D by application of quantum mechanical calculations of chiroptical (ECD and ORD) properties. Assayed by leaf puncture to non-host weeds Chenopodolan D and chenopodolin B showed phytotoxicity while chenisocoumarin and the 9-*O*-acetyl derivative of chenopodolan D were inactive. These results confirm that the nature of the side chain at C- 4 in chenopodolans and in particular its the hydroxylation are important features to impart activity. The activity of chenopodolin B could also be explained by its possible hydrolization into chenopodolin.

Keywords: Chenopodium album; *Phoma chenopodiicola*; phytotoxins; furopyrans; *ent*-pimaradiene; isocoumarines; herbicides

1. Introduction

Fungal pathogens responsible for foliar and stem diseases of *Chenopodium album* L., a worldwide diffused weed of arable crops (Holm et al., 1977) also known as common lambsquarters or fat hen, have been studied both as potential biocontrol agents, and as sources of bioactive metabolites. *Ascochyta caulina* (P. Karst.) v.d. Aa and v. Kest has been first extensively studied for both purposes and, more recently, *Phoma chenopodiicola*. From this latter organism a new phytotoxic unrearranged *ent*-pimaradiene diterpene, named chenopodolin (Cimmino et al., 2013a), and successively three novel tetrasubstituted furopyrans, named chenopodolans A-C (Cimmino et al., 2013b) were recently isolated from its liquid culture; the relation between the structural features and the phytotoxic activity against some weeds was also determined by assaying the natural toxins and some of their hemisynthetic derivatives (Cimmino et al., 2013a; Cimmino et al., 2013b).

A further analysis of the organic extracts of the fungus, aimed both at re-isolating chenopodolans A-C to assign their absolute configuration, and to understand the phytotoxicity of the extracts, higher then that expectable by the content of chenopodolin and chenopodolans A-C, allowed to ascertain the presence of further bioactive metabolites and to identify them.

In particular this manuscript reports on: (a) the isolation and the chemical characterization of three new metabolites produced by *P. chenopodicola*, named chenopodolan D (**1**), chenisocoumarin (**2**) and chenopodolin B (**3**) (Fig. 1); (b) the preliminary studies to evaluate their potential as natural herbicides; (c) the assignment of the absolute configuration of **1** by quantum mechanical calculations of Optical Rotatory Dispersion (ORD) and Electronic Circular Dichroism (ECD), and of **2** by applying an advanced Mosher's method.

2. Results And Discussion

Compounds **1-3** were obtained from the purification of the organic extract of *P. chenopodiicola* as reported in details in the Experimental. Chenopodolan D (**1**, Fig. 1) has the molecular formula

$C_{14}H_{18}O_4$ as deduced by its HR ESIMS spectrum and consistent with six hydrogen deficiencies. Compared to chenopodolans A-C (Cimmino et al., 2013b), its ^{1}H and ^{13}C NMR spectra (Table 1) showed proton and carbon signals very similar to the 2,3,4,6-tetrasubstituted furopyran moiety. Also the signals for the methoxy and the two methyl groups at C-3 , C-2 and C-6, respectively, were very similar to those of the other chenopodolans A-C, while the signals of the side chain attached to C-4 differed substantially. In particular the ^{1}H and ^{13}C NMR spectra showed a broad singlet and a triplet typical of a hydroxymethylene group (HO-CH_2-11) at δ 4.38 (2H)/59.8 (*t*) (Pretsch et al., 2000; Breitmaier and Voelter 1987), instead of the signals of the terminal vinylic methyl group (Me-11) of chenopodolan C (Cimmino et al., 2013b). The presence of a hydroxymethylene is also consistent with the hydroxy group band observed in the IR spectra (Nakanishi and Solomons 1977). These findings suggested for **1** the structure of 11-hydroxychenopodolan C, which was confirmed by the assignment of all the protons and the corresponding carbon chemical shifts based on the couplings observed in the COSY and HSQC spectra (Berger and Braun 2004). Furthermore, the quaternary carbons C-3, C-3a, C-4, C-6, C-7a and C-9 as reported in Table 1 were assigned by the long range couplings observed in the HMBC spectrum (Table 1) (Berger and Braun 2004), Thus chenopodolan D was formulated as 3-(3-methoxy-2,6-dimethyl-7a*H*-furo[2,3-*b*]pyran-4-yl)-but-2-en-1-ol.

This structure was confirmed by all the long range couplings observed in the HMBC spectrum (Table 1) and in particular those between H_2-11 with both C-9 and C-10. Further supports to the structure assigned to **1** were obtained from its HR ESI MS spectrum which showed: the potassium $[2M + K]^+$, sodium [2M + Na] and protonated $[2M + H]^+$ dimmer forms at *m/z* 539, 523 and 501, respectively; the potassium $[M + K]^+$ and sodium $[M + Na]^+$ clusters at *m/z* 289 and 273, respectively; the pseudomolecular ion $[M + H]^+$ *m/z* at 251.1217.

The structure assigned to **1** was finally confirmed by preparing its 11-*O*-acetyl derivative (**4**, Fig. 1) by usual acetylation with pyridine and acetic anhydride. The IR spectrum of **4** showed the absence of any hydroxy group band while its ^{1}H NMR spectrum (Table 1) differed from that of **1**

essentially for the downfield shift (Δδ 0.41 and 0.39) of the H_2C-11 signals resonating as two broad singlets at δ 4.73 and 4.71, respectively, and for the presence of the singlet of the acetyl group at δ 2.08. Its ESIMS spectrum showed potassium $[2M + K]^+$, sodium $[2M + Na]^+$ and protonated $[2M + H]^+$ dimmer forms, potassium cluster $[M + K]^+$ and the pseudomolecular ion $[M + H]^+$ at *m/z*: 623, 607, 585, 331, 293, respectively. Thus, **1** was formulated as 3-(3-methoxy-2,6-dimethyl-7a*H*-furo[2,3-*b*]pyran-4-yl)-but-2-en-1-ol.

The absolute configuration of (-)-**1** was determined by *ab initio* computational analyses of its ORD and ECD spectra (Autschbach, 2009, 2012). This approach was demonstrated to be particularly straightforward and reliable for the absolute configuration assignment of natural products (Mazzeo et al., 2013; Santoro et al., 2013; Santoro et al., 2014), allowing analyses in solution and sometimes on a microscale, using very dilute solutions (Berova et al., 2010). To this end, conformational analysis was carried out on the randomly chosen (*R*)-**1** stereoisomer. The conformational search was first carried out at MM level with MMFF94s force field, then refined by optimization at DFT/B3LYP/TZVP level of theory in gas phase, providing 15 appreciably populated conformers (Fig. S28 and Table S1 in SI). The conformers differ in the rotation of the OCH_3 moiety and of the C4-C9 bond which affect the relative position of the exocyclic double bond in respect to the byciclic system. UV and ECD spectra of (-)-**1** were recorded in THF in the 210-350 nm range (Fig. 2).The UV spectrum shows a maximum at 210 nm (ε 44600), followed by a shoulder at 229 nm (ε 29900), two weak broad bands at 254 nm (ε 11500) and 286 nm (ε 6090) and a very broad band centered at 326 nm (ε 7800). The ECD spectrum shows relatively intense negative Corron effect (CE) at 220 nm (Δε -6.0) followed weaker bands in the low energy spectral range: two positive CEs at 232 nm (Δε +0.4) and 254 (Δε +1.1), a negative band at 272 nm (Δε -0.4) and a broad positive one centred at 288 nm (Δε +0.62)

The UV and ECD spectra of (*R*)-**1**, were then calculated in gas phase at TDDFT/CAM-B3LYP/aug-cc-pVDZ level on previously found conformers and Boltzmann averaged over

conformers populations. Computed ECD spectrum for (*R*)-**1** was then compared with experimental one for (-)-**1** (Fig. 2). Such comparison shows that, although the low energy range of the theoretical spectrum is not in full agreement with the experimental, computations correctly reproduced the strongest Cotton effect at 231 nm in sign and position, suggesting a (*R*) absolute configuration for (-)-**1**. A close look into the ECD spectra of single conformers (Fig. S29) reveals that, although they show quite different ECD spectra, most of them display a negative Cotton effect between 210 and 230 nm, pointing out that the sign of this band can be considered as a reliable probe for absolute configuration assignment of this compound. In order to get a better agreement between computed and experimental ECD spectra, both conformational analysis and ECD calculation were carried out taking into account solvation effects by IEFPCM implicit solvation model (Tomasi et. al., 2005). For this purpose, the outcome from MM conformational analysis on (*R*)-**1** was submitted to optimization at DFT/B3LYP/TZVP theory level by IEFPCM model (THF) leading again to 15 significantly populated conformers (Fig. S28 and Table S1 in SM). As inferred from Table S1 solvent effects give rise to a redistribution of conformers population with decreasing of the most populated conformer 2 and increasing of population of conformers 8 and 11. The UV and ECD spectra for (*R*)-**1** were then calculated at TDDFT/CAM-B3LYP/aug-cc-pVDZ/IEFPCM(THF) level and Boltzmann averaged over conformers populations. Comparison of computed ECD spectrum for (*R*)-**1** with experimental one for (-)-**1** (Fig. 2) shows a better agreement than that with the spectrum computed in gas phase. In fact the IEFPCM computed spectrum better reproduce the low energy spectral range. Thus, when the solvent effects are taken into account the ECD spectral analysis does allow to clearly establish a (*R*) absolute configuration for natural (-)-**1**. The good agreement in position and relative intensity of the ECD CEs with experimental spectrum supports also the accuracy in the theoretical reproduction of conformers population.

To further confirm such configurational assignment computational analysis of ORD curve was then undertaken. The ORD data of (-)-**1** were recorded in $CHCl_3$ at c = 0.2 g/100ml obtaining a plane negative curve (Fig. 3). ORD data for (*R*)-**1** were then calculated on previously found

conformers at TDDFT/B3LYP/aug-cc-pVDZ level in gas phase and Boltzmann averaged over conformers populations. Comparison of computed and experimental data shows (Fig. 3) an agreement in sign, both giving rise to a negative plane curve, thus confirming the assignment of (*R*) absolute configuration for (-)-**1**. However, a difference in one order of magnitude of optical rotation values was observed. To obtain a better numerical agreement between computed and experimental data ORD was calculated also taking into account chloroform solvent effects. Therefore, conformational analysis was carried out by DFT/B3LYP/TZVP/IEFPCM($CHCl_3$) computations, obtaining 14 stable conformers with populations quite similar to those found in THF. For each conformer ORD data were computed at TDDFT/B3LYP/aug-cc-pVDZ/IEFPCM($CHCl_3$) level of theory and Boltzmann averaged over populations, obtaining the ORD curve in Figure 3. As inferred from Figure 3 computations in solution allow to obtain a slightly better numerical agreement with experimental, although with data still one order of magnitude greater than experimental. In conclusion, both ECD and ORD analyses indicate the same assignment of (*R*) absolute configuration for (-)-**1**. However, computed ORD curve does not match (both in gas phase and solvent) the experimental data in order of magnitude.

Chenisocoumarin (**2,** Fig. 1) has the molecular formula $C_{10}H_{10}O_5$, as deduced by its HR ESIMMS and consistent with six hydrogen deficiencies. Its IR spectrum showed bands typical for hydroxy, ester carbonyl and aromatic groups (Nakanishi and Solomons 1977). Compared to that of 6-hydroxymellein, which was previously isolated as the main phytotoxic metabolite from the culture filtrates of the same fungus (Cimmino et al., 2013b), the ^{1}H and ^{13}C NMR spectra (Table 2) of **2** showed very similar signal systems. Indeed, the ^{1}H NMR and COSY spectra showed the presence of two *meta*-coupled aromatic protons (H-6 and H-8) resonating as two doublets (J = 1.7 Hz) at δ 6.35 and 6.33, respectively. Their corresponding carbons were observed at δ 106.8 and 99.2, respectively, and were also assigned for their couplings observed in the HSQC spectrum. Furthermore, the significant signal of the phenolic protons at C-8 hydrogen bonded with the carbonyl group at C-1, previously observed in the ^{1}H NMR spectrum of 6-hydroxymellein, was

absent in **2**. Thus, the two hydroxy phenolic groups were located at C-5 and C-7 also on the basis of the chemical shifts of their corresponding quaternary carbons resonating as two singlets at δ 164.1 and 155.3 (C-7 and C-5, respectively) (Breitmaier and Voelter 1987). These latter were assigned also on the basis of the couplings observed in the HMBC spectrum (see Table 2), as well as the other quaternary carbons at δ 142.5, 135.8 and 169.0, which were assigned to C-4a, C-8a and the carbonyl group C-1, respectively. Furthermore, the signal systems typical for 4-hydroxymellein were observed in the ^{1}H and ^{13}C NMR spectra (Table 2) at δ 4.57 (H-3, *dq*, *J* = 6.6 and 1.8 Hz)/67.2(C-3, *d*), 4.38 (H-4, *d*, J = 1.8 Hz)/77.5(C-4, *d*) and 1.48 (Me-9, *d*, *J* = 6.6 Hz)/15.8 (Me-19, *q*).

Based on these findings, **2** was formulated as 4,5,7-trihydroxy-3-methyl-isochroman-1-one. This structure was supported from all the couplings observed in the HMBC spectrum (Table 2) and the data obtained from its HR ESIMS spectrum. This latter showed the sodium cluster $[M + Na]^+$ and the pseudomolecular ion $[M + H]^+$ at *m/z* 233 and 211.1218, respectively. The *trans* relative configuration was assigned to **2** on the basis of the significant correlation observed in its NOESY spectrum between H-3 and Me-9, (Berger and Braun 2004).

The absolute configuration of **2** was assigned by applying an advanced Mosher's method (Othani et al, 1991). Besides the suitable secondary hydroxyl group at C-3, **2** also contained two phenol hydroxy groups at C-5 and C-7. First, **2** was converted into the corresponding 5,7-*O,O'*-dimethyl derivative **5** by treatment with an ethereal solution of diazomethane. **5** showed the significant presence of the hydroxy group into the IR spectrum (Nakanishi and Solomon, 1987), while its ^{1}H NMR spectrum differed from that of **2** for the presence of the two singlets typical of methoxy groups at δ 3.92 and 3.89, respectively (Pretsch et al., 2000). Its ESI MS spectrum showed: the potassium $[2M + K]^+$ and the sodium $[2M + Na]^+$ dimeric forms at *m/z* 515, 499, respectively; the potassium $[M + K]^+$ and sodium $[M + Na]^+$ clusters at *m/z* 277, 261, respectively; and the pseudomolecular ion $[M + H]^+$ at *m/z* 239. By reaction with *R*-(-)-α-methoxy-α-trifluoromethylphenylacetyl (MTPA) and *S*-(+)MTPA chlorides, **5** was converted into the

corresponding diastereomeric *S*-MTPA and *R*-MTPA monoesters at C-4 (**6** and **7**, respectively), whose spectroscopic data were consistent with the structure assigned to **2**. Subtracting the chemical shift of the protons (Table 3) of the 3-*O*-*R*-MTPA (**7**) from that of 3-*O*-*S*-MTPA (**6**) esters, the Δδ (**6**-**7**) values for all of the protons were determined as reported in Figure 4. The positive Δδ values were located on the right-hand side, and those with negative values on the left-hand side of the model A as reported in Othani et al. (1991). This model allowed the assignment of the *R* configuration at C-4. Considering the relative configuration assigned by NMR as above reported, **2** was formulated as (4*R*,3*S*)-4,5,7-trihydroxy-3-methyl-isochroman-1-one.

Chenopodolin B (**3**) had a molecular formula of $C_{26}H_{32}O_9$ as deduced by its HR ESI MS spectrum and consistent with eleven hydrogen deficiencies. The preliminary investigation of its ^{1}H and ^{13}C NMR spectra (Table 4) showed that they are very similar to those of chenopodolin (Cimmino et al., 2013a). Indeed **3** showed the signal systems typical of the tetracyclic *ent*-pimaradiene lactone and also those corresponding to the α,β-unstaturated ketone at C(6)-C(8), the vinylic and the tertiary methyl both bonded to C-13, as well as the acetoxy groups at C-1 and C-12. The only difference observed by the comparison of the above cited spectra was the downfield shift (Δδ 1.07) of the proton of C-3, appearing as broad singlet at δ 5.21 while its corresponding carbon resonated at δ 78.1. The singlet of a further acetyl group was observed at δ 2.10 (MeCO, *s*)/174.8 (MeCO, s) and 20.7 (MeCO, *q*). Thus, **3** appeared to be the 3-*O*-acetyl chenopodolin for which the chemical shifts of all the protons and the corresponding carbons were assigned on the basis of the couplings observed in the COSY, HSQC and HMBC spectra (Table 4) and the NOESY spectrum. In fact in this latter spectrum significant correlations were observed between H-15 with both H_2-16 and Me-17, H-9 with H-3, and H-12 and H_2-11 and Me-17. The structure assigned to **3** was supported by the data obtained from its HR ESIMS spectrum, which showed the sodium dimmer form $[2M + Na]^+$ and the sodiated cluster $[M + Na]^+$ at *m/z* 999 and 511.1953, respectively. When compared to the chenopodolin 1-*O*-acetyl derivative prepared by its usual acetylation with pyridine and acetic anhydride (Cimmino et al., 2013a), **3** showed the same chromatographic behaviour, also

when eluted in mixture, by TLC analysis solvent systems A and C) and the same ^{1}H NMR data as previously reported (Cimmino et al., 2013a). Thus, **3** was formulated as (1*S*,2*S*,3*S*,4*S*,5*S*,9*R*,10*S*,12*S*,13*S*)-1,3,12-triacetoxy-2,-6-oxo-*ent*-pimara-7(8),15-dien-18-oic acid 2,18-lactone. This is the first isolation of **3** as a naturally occurring compound. It was not an artefact generated by the transesterification of chenopodolin with ethyl acetate during the extraction process because chenopodolin remained unaltered when dissolved and left in EtOAc (the solvent used to extract the fungal culture filtrates) for 2-3 days at room temperature.

Assayed at $4x10^{-3}$ M on punctured detached leaves, **3** proved to be active in particular on *Sonchus arvensis*, causing the fast appearance of wide necrosis (scored +++) and on *Urtica dioica* and *Parietaria officinalis*, with smaller but still evident necrosis (+). This result differed from the not toxic activity previously observed when **3** was tested on different plants *(Mercurialis annua*, *Cirsium arvense* and *Setaria viride*) using the same bioassay (Cimmino et al., 2013a). The different behaviour could be due to different plant sensitivity. Furthermore, it is also important to consider that when **3** crosses the plant cell membrane it could be partially or fully hydrolized at the physiological pH, according to the well know lethal metabolism (Hassal, 1990), into chenopodolin. Compound **1** was less toxic compared to **3**, as it caused medium-size necrosis (++) on *Stellaria media* and *U. dioica*, whereas was inactive against other plants. Finally, both 9-*O*-acetyl chenopodolan D (**4**) and chenisocoumarin (**2**) proved to be inactive on all the tested plants. The phytotoxicity observed for **1** was in agreement with the results previously obtained testing chenopodolans A-C (Cimmino et al., 2013b) confirming that the nature of the side chain at C- 4, and in particular its hydroxylation, is an important feature to impart biological activity. Its 9-*O* acetyl derivative probably is inactive because it is not completely hydrolized into **1**.

In conclusion, a new furopyran, named chenopodolan D (**1**), a new isocoumarin, named chenisocoumarin (**2**) and a new unrearranged *ent*-pimaradiene, named chenopodolin B (**3**), were isolated from *P. chenopodiicola*, a fungal pathogen proposed for the biocontrol of *C. album*. The absolute configuration of **1** was established by quantum mechanical calculations of ECD and ORD

spectra, while that of **2** by applying an advanced Mosher's method. Both **1** and **3** showed phytotoxic activity. So that it is possible also hypothesised a synergism between them and chenopodolin and chenopodolans B and C which contribute to the phytoxicity showed by the culture filtrates of *P. chenopodiicola* and its organic extracts. This could be an important finding in the view of a practical application as herbicides of these phytotoxic metabolites in the management of *C. album* .

3. EXPERIMENTAL

3.1. General

Optical rotations were measured in $CHCl_3$ on Jasco P-1010 and Jasco DIP-370 digital polarimeters; absorption and ECD spectra were recorded at room temperature on a JASCO J815 spectropolarimeter, using 0.5 mm cells and concentrations of about 1×10^{-3} M. IR spectra were recorded as glassy film on a Perkin-Elmer Spectrum One FT-IR Spectrometer and UV spectra were recorded in MeOH solution on a Perkin-Elmer Lambda 25 UV/Vis spectrophotometer. ^{1}H and ^{13}C NMR spectra were recorded at 400/100 MHz in $CDCl_3$ on Bruker spectrometers. The same solvent was used as internal standard. Carbon multiplicities were determined by DEPT spectra (Berger and Braun, 2004) DEPT, COSY-45, HSQC, HMBC and NOESY experiments (Berger and Braun, 2004) were performed using Bruker microprograms. HRESI and ESIMS spectra were recorded on Waters Micromass Q-TOF Micro and Agilent Technologies 6120 Quadrupole LC/MS instruments, respectively. Analytical and preparative TLC were performed on silica gel plates (Merck, Kieselgel 60 F_{254}, 0.25); or reverse phase (Whatman, Stratocrom RP-18, 0.20 mm) the spots were visualized by exposure to UV light and/or by spraying first with 10% H_2SO_4 in MeOH and then with 5% phosphomolybdic acid in EtOH, followed by heating at 110 °C for 10 min. Column chromatography was performed on silica gel (Merck, Kieselgel 60, 0.063-0.200 mm). Solvent systems: (A) $CHCl_3$-*i*-PrOH (97:3); (B) EtOH-H_2O (6:4); (C) $CHCl_3$-*i*-PrOH (95:5); (D) *n*-hexane-Me_2CO (7:3); (E) *n*-hexane-Me_2CO (1:1).

3.2. Fungal strain.

The fungus was isolated from diseased leaves of *C. album* and identified as *P. chenopodiicola* (Berestetskyi, unpublished). A monoconidial isolate was deposited in the culture collection of both the All-Russian Research Institute of Plant Protection, Pushkin, Saint-Petersburg, Russia (I-13.2) and the Institute of Sciences of Food Production, Bari, Italy (ITEM 12534). The isolate was routinely grown and maintained in plates and slants containing potato-dextrose agar (PDA, Sigma-Aldrich, Chemie Gmbh, Buchs, Switzerland).

*3.3. Production, Extraction and Purification of chenopodolan D, chenisocumarine and chenopodolin B (**1**-**3**).*

The fungus was grown in 1 l Erlenmeyer flasks containing 300 mL of a defined mineral medium (Pinkerton and Strobel, 1976) as recently described (Cimmino et al., 2013b). The culture filtrates (4.6 l) were lyophilized, dissolved in distilled water (1/10 of its original volume) and then extracted by EtOAc (4 x 1 l). The organic extract (780 mg), having high phytotoxic activity, was fractionated by CC eluted with the solvent system A, as already described (Cimmino et al., 2013b). Six homogeneous fraction groups were collected. The residue (43.3 mg) of the fourth fraction was further purified by preparative TLC, eluted with the solvent system A, giving five fractions. The residue of the second fraction, obtained as a yellow oil, was identified as chenisocumarin (**2**, *R*f 0.24, 7.8 mg, 1.69 mg/l). The residue (11 mg) of the third fraction was further purified by reverse phase TLC (eluent system B) yielding a yellow oil identified as chenopodolan D (**1**, *R*f 0.66, 4.5 mg, 0.98 mg/l). The residue (138.7 mg) of the second fraction of the original column was purified by CC eluted with the system C, yielding five homogeneous fractions. The residue (67.6 mg) of the second fraction was washed with *n*-hexane followed by $CHCl_3$ to separated 6-hydroxymellein. The residue (4.9 mg) was further purified by preparative TLC (eluent system D) obtaining a white amorphous solid, which was identified as chenopodolin B (**3**, *R*f 0.41, 4 mg, 0.85 mg/l).

*3.4. Chenopodolan D (**1**)*

Compound **1: .** $[\alpha]^{25}_{D}$: -6.8 (*c* = 0.19); IRν_{max} 3324, 1733, 1656, 1622, 1545, 1465, 1354, 1243 cm^{-1}; UV λ_{max} nm (log ε) 337 (3.6), 252 (sh); ^{1}H and ^{13}C NMR spectra: see Table 1; HRESI MS (+) *m/z*: 539 $[2M + K]^+$, 523 $[2M + Na]^+$, 501 $[2M + H]^+$, 289 $[M + K]^+$, 273 $[M + Na]^+$, 251.1217 $[M + H]^+$ (calcd for $C_{14}H_{18}O_4$ 251.1208).

*3.5. Chenisocoumarin (**2**)*

Compound **2:** $[\alpha]^{25}_{D}$: -1.6 (*c* = 0.36, MeOH); IRν_{max} 3153, 1625, 1500, 1461, 1374 cm^{-1}; UV λ_{max} nm (log ε) 303 (3.6), 266 (4.1), 229 (sh); ^{1}H and ^{13}C NMR spectra: see Table 2; HRESI MS (+) 233 $[M + Na]^+$, 211.1218 $[M + H]^+$ (calcd for $C_{10}H_{10}O_5$ 211.1208).

*3.6. Chenopodolin B (**3**)*

Compound **3**: $[\alpha]^{25}_{D}$: -55.5 (*c* = 0.20); IR ν_{max} 1798, 1719, 1460, 1368, 1269, 1233 cm^{-1}; UV λ_{max} nm (log ε) 277 (3.2), 229 (3.8); ^{1}H and ^{13}C NMR spectra: see Table 4; HRESI MS (+) *m/z*: 999 $[2M + Na]^+$, 511.1953 $[M + Na]^+$ (calcd for $C_{26}H_{32}NaO_9$ 511.1944).

*3.7. 11-O-acetylchenopodolan D (**4**)*

Chenopodolan D (**1**, 2.5 mg) was acetylated with pyridine (50 μl) and Ac_2O (50 μl) at room temperature for 1 h. The reaction was stopped by the addition of MeOH and the azeotrope, obtained by the addition of benzene, was evaporated by an N_2 stream. The oily residue (5.0 mg) was purified by preparative TLC eluted with the solvent system E, to give the 11-*O*-acetyl derivative **4** of chenopodolan D as a homogeneous compound (*R*f 0.62, 2.4 mg). Derivative **4** had: IR ν_{max} 1732, 1689, 1622, 1551, 1459, 1370, 1232 cm^{-1}; UV λ_{max} nm (log ε) 336 (3.4), 253 (3.6); ^{1}H and ^{13}C NMR spectra: see Table 1. HRESI MS (+) *m/z*: 623 $[2M + K]^+$, 607 $[2M + Na]^+$, 585 $[2M + H]^+$, 331 $[M + K]^+$, 293 $[M + H]^+$.

*3.8. 5,7-O,O'dimethylchenisocoumarin (**5**)*

Chenisocoumarin (**2**, 4 mg), dissolved CH_3OH (2 ml) was added with an ethereal solution of diazomethane (200 μl). The reaction was carried out overnight at room temperature in the dark. The reaction was stopped by evaporation under N_2 stream. The residue (7.6 mg) was purified by TLC, eluted with the solvent system A, yielding the 5,7-*O*,*O*'-demethyl derivative of **2** (**5**) as an homogeneous compound (2.6 mg, *R*f 0.46). Derivative **5** had: IR ν_{max} 3406, 1698, 1604, 1560 cm^{-1}; UV λ_{max} nm (log ε) 299 (3.5), 262 (4.2), 230 (sh); ^1H and ^{13}C NMR spectra: see Table 2. ESIMS (+) *m/z*: 515 $[2M + K]^+$, 499 $[2M + Na]^+$, 277 $[M + K]^+$, 261 $[M + Na]^+$, 239 $[M + H]^+$.

*3.9. 11-O-(S)-α-Methoxy-α-trifluoromethyl-α-phenylacetate (MTPA) Ester of **5** (**6**)*

(*R*)-(-)-MPTA-Cl (20 μl) was added to **5** (1.0 mg) dissolved in dry pyridine (20 μl). The mixture was kept at room temperature for 1 h and then the reaction stopped by adding MeOH. Pyridine was removed by a N_2 stream. The residue (2.5 mg) was purified by preparative TLC, eluted with the solvent system D, yielding **6** as a homogeneous oil (*R*f 0.71, 1.2 mg). It had: IR ν_{max} 1722, 1606, 1581 cm^{-1}; UV λ_{max} nm (log ε) 301 (3.9), 261 (4.3), 232 (sh); ^1H NMR spectrum see Table 3; ESIMS (+) *m/z*: 947 $[2M + K]^+$, 931 $[2M + Na]^+$, 493 $[M + K]^+$, 477 $[M + Na]^+$, 455 $[M + H]^+$.

*3.10. 11-O-(R)-α-Methoxy-α-trifluoromethyl-α-phenylacetate (MTPA) Ester of **5** (**7**)*

(*S*)-(+)-MPTA-Cl (20 μl) was added to **5** (1.0 mg) dissolved in dry pyridine (20 μl). The reaction was carried out under the same conditions used for preparing **6** from **5**. The purification of the crude residue (2.2 mg) by preparative TLC eluted with solvent system D, allowed to obtain **7** as a homogeneous oil (*R*f 0.71, 1.2 mg). It had: IR ν_{max} 1720, 1605, 1581 cm^{-1}; UV λ_{max} nm (log

ε) 303 (3.9), 262 (4.2), 229 (sh); ^{1}H NMR spectrum see Table 3; ESIMS (+) *m/z*: 947 $[2M + K]^+$, 931 $[2M + Na]^+$, 493 $[M + K]^+$, 477 $[M + Na]^+$, 455 $[M + H]^+$.

3.11. Computational methods

Preliminary conformational analysis was performed by Spartan02 package (SPARTAN 02) employing MMFF94s molecular mechanics (MM) force field with Monte Carlo searching and assuming the (*R*) absolute configuration for **1**. All possible conformers were searched, considering the degrees of freedom of the system within a range of 30 kcal/mol and retaining only the structures in an energy range of 10 kcal/mol with respect to the most stable one. The minimum energy conformers found by MM were further fully optimized by Gaussian09 package (Frisch et al., 2009) using the Density Functional Theory (DFT) at the DFT/B3LYP/TZVP level either in gas phase or in THF and $CHCl_3$ by IEFPCM solvation model (Tomasi et. al. 2005). All conformers are real minima, no imaginary vibrational frequencies have been found and the free energy values have been calculated and used to get the Boltzmann population of conformers at 298.15 K. The DFT geometries were then employed as input for Time Dependent DFT (TDDFT) calculations of UV, ECD, and ORD spectra both in gas phase and by IEFPCM implicit solvation model in THF and $CHCl_3$. Optical rotations were computed by using the TDDFT/B3LYP/aug-cc-pVDZ level on the DFT optimized geometries. The latter were also employed as input geometries for calculation of UV and ECD spectra at the TDDFT/CAM-B3LYP/aug-cc-pVDZ level and taking into account the lowest 30 states. TDDFT calculations employing the long-range corrected CAM-B3LYP functional (Yanai et al., 2004) provided good reproduction of Cotton effects observed in the theoretical ECD spectra (Evidente et. al., 2011). The theoretical ORD, UV, and ECD spectra were obtained as average over the conformers Boltzmann populations. The ECD spectra were obtained from calculated excitation energies and rotational strengths, as a sum of Gaussian functions centered at the wavelength of each transition, with a parameter σ (width of the band at ½ height) of 0.2 eV using SpecDis v1.60 program (Bruhn et al., 2013). The ECD spectrum was also calculated both in

the length and velocity formalisms to guarantee origin independence and to evaluate the quality of the molecular wave functions employed (Moscowitz, 1965). These calculated spectra were almost coincident, indicating a good level of calculation. Therefore, in all figures only the velocity-form predicted spectra are reported.

3.12. Leaf puncture assay

Each metabolite was first dissolved in MeOH and then diluted with distilled water to the desired concentrations (final concentration of methanol: 2%). The compounds were tested by using a leaf puncture assay on 6 different plant species, namely *Stellaria media*, *Urtica dioica*, *Sonchus arvensis*, *Parietaria officinalis*, *Lactuca serriola*, *Helianthus annuus*, with the weedy plants (the first four in the list) collected in local open fields, and the crop plants grown in pots. Pure compounds were tested at 4×10^{-3} M by applying a droplet (20 µl) of solution to detached leaves previously punctured with a needle. Five replications were used for each metabolite and for each plant species tested. Leaves were kept in a moistened chamber under continuous fluorescent lights. Symptoms were estimated visually between three to five days after droplet application, by using a visual scale from 0 (no symptoms) to 4 (necrosis wider than 1 cm). Control treatments were carried out by applying droplets not containing the metabolites.

Acnowledgements

This research was carried out in part in the frame of Programme STAR, financially supported by UniNA and Compagnia di San Paolo. Prof. A. Evidente is associated to the "Istituto di Chimica Biomolecolare del CNR, Pozzuoli, Italy".

Appendix A. Supplementary material

Supplementary data associated with this article can be found, in the online version at htpp//:……

References

Autschbach, J., 2009. Computing chiroptical properties with first-principles theoretical methods: background and illustrative examples. Chirality 21, 116–152.

Autschbach, J., 2012. *Ab initio* electronic circular dichroism and optical rotatory dispersion: from organic molecules to transition metal complexes, in: Berova, N., Polavarapu, P.L., Nakanishi, K., Woody, R.W., (Eds.), Comprehensive Chiroptical Spectroscopy: Applications in Stereochemical Analysis of Synthetic Compounds, Natural Products, and Biomolecules. John Wiley & Sons, Inc., Hoboken, NJ, USA. Vol. 1, Chapter 21, pp. 593–642.

Berger, S., Braun, S., 2004. 200 and More Basic NMR Experiments: a Practical Course, first ed. Wiley-VCH, Weinheim.

Berova, N., Ellestad, G.A., Harada. N., 2010. Characterization by circular dichroism spectroscopy, in: Mander, L., Lui, H.-W. (Eds.), Comprehensive natural products II. Chemistry and Biology. Elsevier, Oxford, Vol. 9, Chapter 4, pp. 91–146.

Breitmaier, E., Voelter, W., 1987. Carbon-13 NMR Spectroscopy, VCH, Weinheim, pp. 183-280.

Bruhn, T. et al., 2013. SpecDis: Quantifying the comparison of calculated and experimental electronic circular dichroism spectra. Chirality 25, 243–249.

Cimmino, A. et al., 2013a. Chenopodolin: a phytotoxic unrearranged *ent*-pimaradiene diterpene produced by *Phoma chenopodiicola, a* fungal pathogen for *Chenopodium album* biocontrol. J. Nat. Prod. 76, 1291-1297.

Cimmino, A. et al., 2013b. Chenopodolans A-C: phytotoxic furopyrans produced by *Phoma chenopodiicola,* a fungal pathogen of *Chenopodium album*. Phytochemistry 96, 208-213

Evidente, A. et al., 2011. Regiolone and isosclerone, two enantiomeric phytotoxic naphthalenone pentaketides: computational assignment of absolute configuration and its relationship with phytotoxic activity. Eur. J. Org. Chem. 5564−5570.

Frisch, M.J. et al., 2009. Gaussian 09, Revision A.02, Gaussian, Inc., Wallingford, CT.

Hassal, K.A., 1990. Biochemistry and Use of Pesticides, Verlag Chemie, Weinheim, pp 58, 72, 304, 429, 497.

Holm, L.G. et al., 1997. The World's Worst Weeds (Distribution and Biology), University Press of Hawaii, Honoloulou, pp. 84-91.

Mazzeo, G. et al., 2013. Absolute configurations of fungal and plant metabolites by chiroptical methods. ORD, ECD, and VCD studies on phyllostin, scytolide, and oxysporone. J. Nat. Prod. 76, 588-599.

Moscowitz, A., 1965. Action of light and organic crystals. In: Sinanoglu, O. (Eds.), Modern quantum chemistry, Part III, Academic Press, London, pp. 31.

Nakanishi, K., Solomon, P. H., 1977. Infrared Absorption Spectroscopy, second ed. Holden Day, Oakland, pp. 17-44.

Pinkerton, F., Strobel, G.A., 1976. Serinol as an activator of toxin production in attenuated cultures of *Helminthosporium sacchari*. Proc. Natl. Acad. Sci. U.S.A. 73, 4007-4011.

Pretsch, E., Bühlmann, P., Affolter, C., 2000. Structure Determination of Organic Compounds - Tables of Spectral Data, Springer-Verlag, Berlin, pp. 161-243.

Ohtani, I. et al., 1989. An application of an advanced Mosher's method. Tetrahedron 30, 3147-3150.

Santoro, S. et al., 2013. Agarsenone, a cadinane sesquiterpenoid from *Commiphora erythraea*. J. Nat. Prod. 76, 1254-59.

Santoro, E. et al., 2014. Absolute configuration of bioactive furanogermacrenones from *Commiphora erythraea* (Ehrenb) Engl. by computational analysis of their chiroptical properties. Tetrahedron 70, 8033-8039.

SPARTAN '02; Wavefunction Inc.: Irvine, CA; http://www.wavefunction.com.

Tomasi, J., Mennucci, B., Cammi, R., 2005. Quantum mechanical continuum solvation models. Chem. Rev. 105, 2999-3094.

Yanai, T., Tew, D.P., Handy, N.C.,. 2004. A new hybrid exchange–correlation functional using the Coulomb-attenuating method (CAM-B3LYP). Chem. Phys. Lett. 393, 51-57.

Table 1.
^{1}H and ^{13}C NMR data of chenopodolan D (**1**) and 1H NMR data of its 11-*O*-acetylderivative (**4**)[a,b]

Position	**1**			4
	δC[c]	δH (*J* in Hz)	HMBC	δH (*J* in Hz)
2	163.5 *s*		Me-8	
3	165.9 *s*		H-7a, OMe, Me-8	
3a	101.9 *s*		H-7a, Me-8	
4	126.2 *s*		H-7a, Me-13	
5	135.7 *d*	6.98 *s*	Me-13	6.96 *s*
6	160.1 *s*		H-5, H-7a, Me-13	
7a	93.7 *d*	6.18 *s*		6.19 *s*
8	14.4 *q*	1.95 (3H) *s*		1.93 (3H) *s*
9	135.9 *q*		H-10, H_2-11, Me-12	
10	131.7 *d*	5.68 *br t (J* = 6.6)[d]	H_2-11	
11	59.8 *t*	4.32 (2H) *br s*		4.73 *br s*
				4.71 *br s*
12	16.5 *q*	1.85 (3H) *s*[d]	H-10	1.88 (3H) *s*
13	13.7 *q*	2.05 (3H) *s*	H-5	2.04 (3H) *s*
OMe	56.1 *q*	3.92 *s*		3.92 (3H) *s*
MeCO				2.08 (3H) *s*

[a]The chemical shifts are in δ values (ppm) from TMS. [b]2D ^{1}H, ^{1}H (COSY) ^{13}C, ^{1}H (HSQC) NMR experiments delineated the correlations of all the protons and the corresponding carbons. [c]Multiplicities were assigned by DEPT spectrum. [d]Allylic coupling (< 1 Hz) was observed in the COSY spectrum between H-10 and Me-12

Table 2
^{1}H and ^{13}C NMR data of chenisocoumarin (**2**)[a,b] and its .5,7-*O,O'*-dimethyl derivative (**5**)

Position	**2**			**5**
	δC[c]	δH (*J* in Hz)	HMBC	δH (*J* in Hz)
1	169.0 *s*		H-8, H-3, Me-9	
3	67.2 *d*	4.57 *dq* (6.6, 1.8)	H-3, Me-9	4.54 *dq* (6.6, 1.3)
4	77.5 d	4.38 d (1.8)	Me-9	4.47 *d* (1.3)
4a	142.5 *s*		H-4, H-3	
5	155.3 *s*		H-6, H-4	
6	106.8 *d*	6.35 *d* (1.7)	H-8, H-4	6.54 *br s*
7	164.1 s		H-8	
8	99.2 s	6.33 *d* (1.7)	H-6, H-4	6.50 *br s*
8a	135.8 s			
9	15.8 q	1.48 (3H) *d* (6.6)	H-4, H-3,	1.50 (3H) *d* (6.6)
OMe				3.92 (3H) *s*
OMe				3.89 (3H) *s*

[a]The chemical shifts are in δ values (ppm) from TMS. [b]2D ^{1}H, ^{1}H (COSY) ^{13}C, ^{1}H (HSQC) NMR experiments delineated the correlations of all the protons and the corresponding carbons. [c]Multiplicities were assigned by DEPT spectrum.

Table 3
^{1}H NMR data of 4-*O*- (*S*)- and 4-*O*- (*R*)-MTPA esters of chenisocumarine 5,7-*O,O'*-dimetilderivative (**6** and **7**, respectively)

	6	**7**
	δ (H (*J* in Hz)	δ (H (*J* in Hz)
3	4.702 *br q* (6.5)	4.661 *br q* (6.7)
4	5.945 *br s*	5.907 *br s*
6	6.637 *br s*	6.694 *br s*
8	6.544 *br s*	6.578 *br s*
9	1.448 (3H) *d* (6.5)	1.417 (3H) *d* (6.7)
OMe[a]	3.920 (3H) *s*	3.945 (3H) *s*
OMe[a]	3.870 (3H) *s*	3.874 (3H) *s*
OMe	3.430 (3H) *s*	3.371 (3H) *s*
Ph	7.381-7.312 *m*	7.414-7.307 *m*

[a]These assignments can be reversed

Table 4. ^{1}H and ^{13}C NMR Data of chenopodolin B (**3**)[a,b]

Position	δC[c]	δH (*J* in Hz)	HMBC
1	72.4 *d*	5.07 (1H) *d* (4.9)	Me-20
2	76.9 *d*	4.62 (1H) d (4.9)	H-1, Me-19
3	78.1 *d*	5.21 (1H) *br s*	H-5, H-1
4	46.7 *s*		H-5, Me-19
5	58.7 *d*	2.96 (1H) *s*	H-1, H-3, Me-19
6	194.2 *s*		H-5
7	126.7 *d*	5.85 (1H) *s*	H_2-14
8	155.7 *s*		H_2-14, H_2-11, H-9
9	48. *d*	3.00 (1H) *m*	
10	42.1 s		H-5, H-2, Me-20
11	11.9 *t*	1.43 (2H) *m*	Me-20
12	76.8 *d*	4.71 (1H) *t*	H-14, H_2-11, Me-17
13	41.5 *s*		H_2-16, H_2-14, Me-17
14	43.3 *t*	2.73 (1H) d (16.0)	Me-17
		2.31 (1H) *d* (16.0)	
15	139.3 *d*	5.87 (1H) *dd* (17.8,11.2)	H-16B, H_2-14, H-12, Me-17
16	116.8 *t*	5.19 (1H) *d* (11.2)	Me-17
		5.03 (1H) *d* (17.8)	
17	25.5 *q*	1.08 (3H) *s*	H-12
18	175.4 *s*		H-5, H-3, Me-19
19	12.1 *q*	1.47 (3H) *s*	H-5
20	17.3 *q*	1.12 (3H) *s*	H-1, H-5
Me<u>CO</u>-12	170.6 s		H-12, <u>Me</u>CO-12
Me<u>CO</u>-3	174.8 s		H-5, H-1, H-2, Me-19
Me<u>CO</u>-1	169.4 s		H-1, <u>Me</u>CO-1
<u>Me</u>CO-1	20.1 q	2.27 (3H) *s*	
<u>Me</u>CO-3	20.7 q	2.10 (3H) *s*	
<u>Me</u>CO-12	20.7 q	2.07 (3H) *s*	

[a]The chemical shifts are in δ values (ppm) from TMS. [b]2D ^{1}H, ^{1}H (COSY) ^{13}C, ^{1}H (HSQC) NMR experiments delineated the correlations of all the protons and the corresponding carbons. [c]Multiplicities were assigned by DEPT spectrum.

Figure Legend

Fig. 1. Structures of: chenopodolan D (**1**) chenisocoumarin (**2**) chenopodolin B (**3**), 11-*O*-acetyl-chenopodolan D (**4**), 5,7-*O,O'*-dimetilderivative-, 4-*O*-*S*-MTPA- and 4-*O*-*R*-MTPA esters of chenisocoumarin (**5, 6** and **7**, respectively).

Fig. 2. Experimental UV and ECD spectra of (-)-**1** [solid red line, THF] and calculated UV and ECD spectra for (*R*)-**1** [TDDFT/CAM-B3LYP/aug-cc-pVDZ//DFT/B3LYP/TZVP/gas phase dotted green line; TDDFT/CAM-B3LYP/aug-cc-pVDZ//DFT/B3LYP/TZVP/IEFPCM(THF) dashed blue line; 0.2 eV bandwidth]. Calculated UV and ECD spectra are blue shifted of +20.0 nm and reduced 20 times.

Fig. 3. Experimental ORD curve of (-)-**1** [solid red line (♦), $CHCl_3$] and calculated ORD for (*R*)-**1** [TDDFT/CAM-B3LYP/aug-cc-pVDZ//DFT/B3LYP/TZVP/gas phase, dotted green line (▲); TDDFT/CAM-B3LYP/aug-cc-pVDZ//DFT/B3LYP/TZVP/IEFPCM($CHCl_3$), dashed blue line (●)].

Fig. 4. Structures of 4-*O*-S- and 4-*O*-R-MTPA esters of 5,7-*O,O'*-dimethyl chenisocoumarin. (**6** and **7**, respectively), reporting the Δδ value obtained by comparison (**6**-**7**) of each proton system.

Figure 1

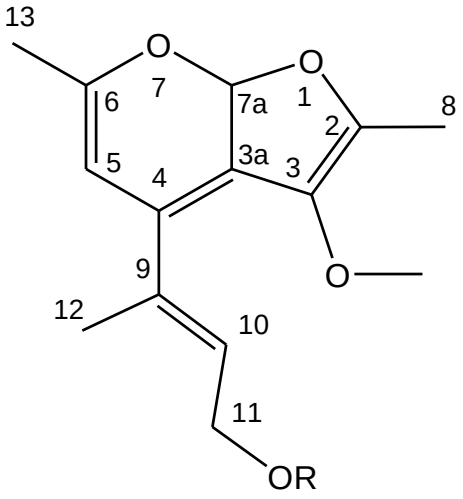

1 R=H
4 R=Ac

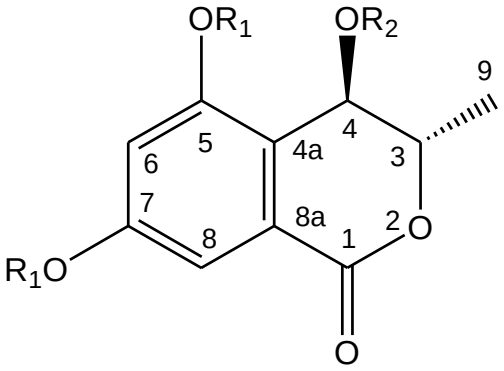

2 R_1= H, R_2= H
5 R_1= CH_3,R_2= H
6 R_1= CH_3, R_2= *S*-MPTA
7 R_1= CH_3, R_2= *R*-MPTA

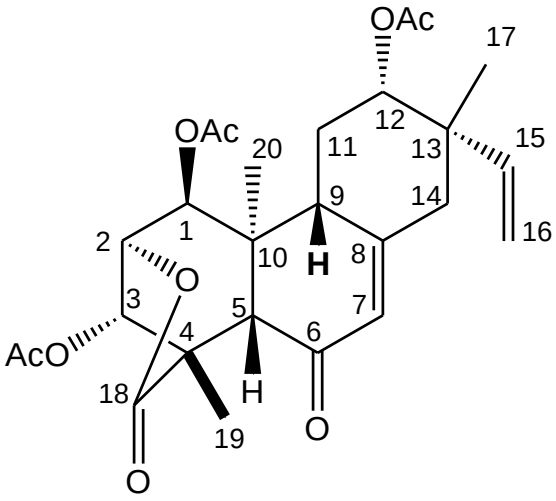

3

Figure. 2

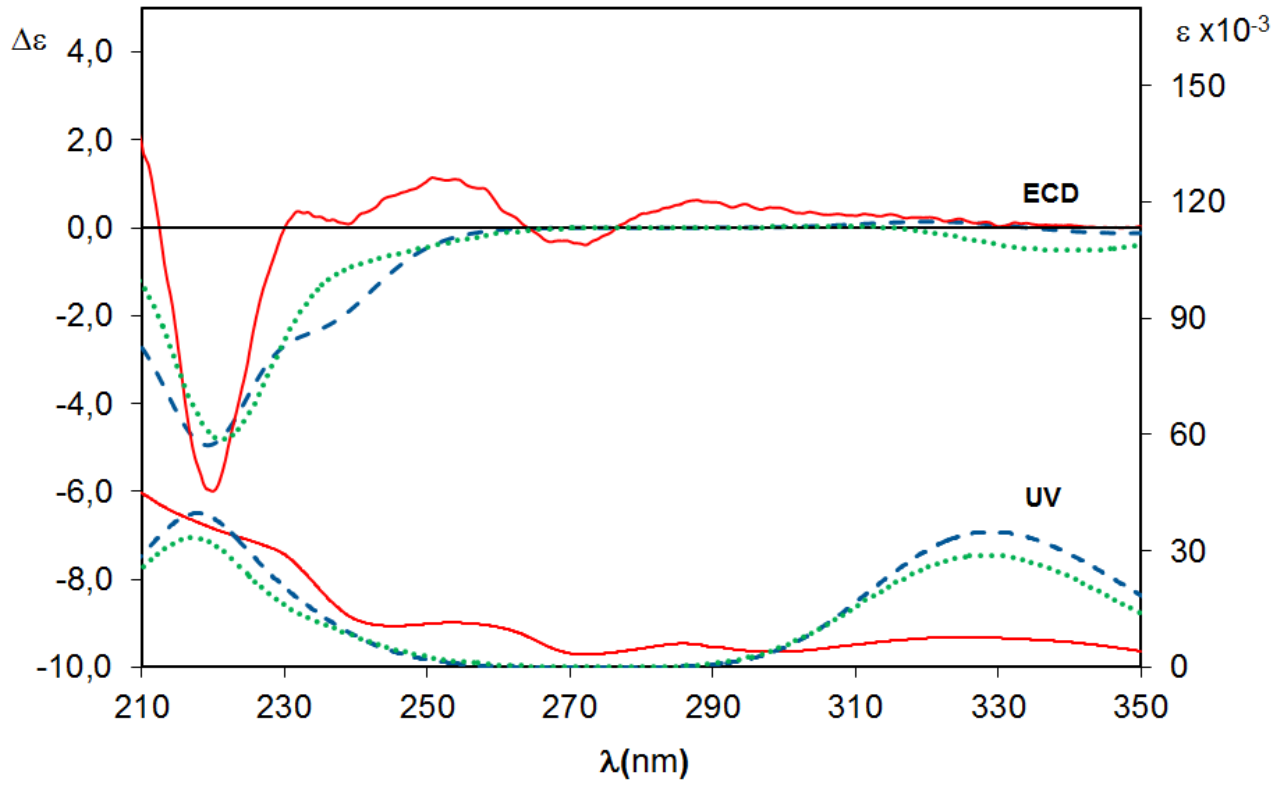
Δε
4,0
2,0
0,0
-2,0
-4,0
-6,0
-8,0
-10,0
ε x10-3
150
120
90
60
30
0
ECD
UV
210
230
250
270
290
310
330
350
λ(nm)

Figure. 3

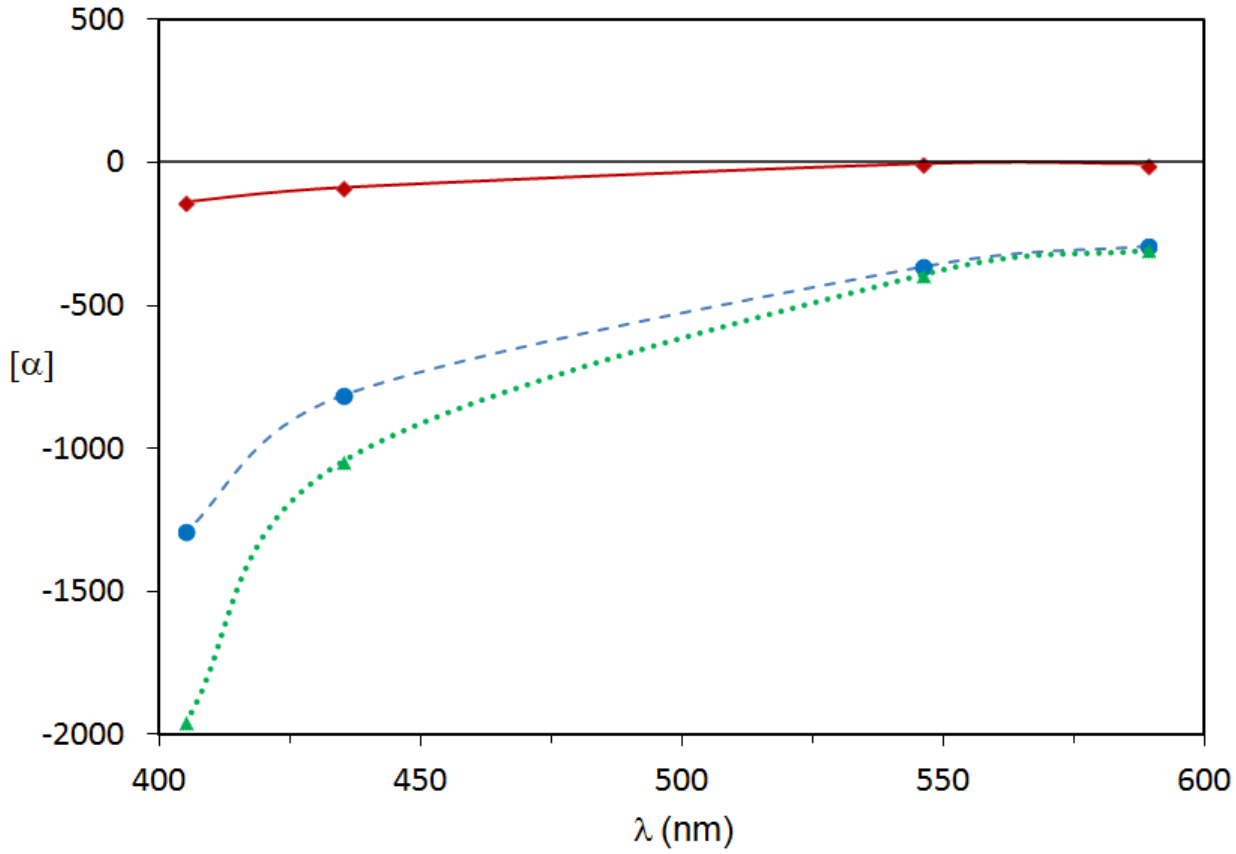

Fig. 4

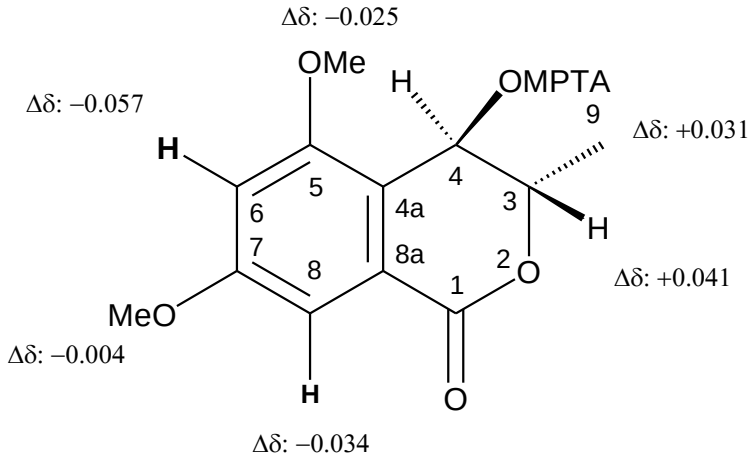
Δδ: −0.025
OMe
H
OMPTA
Δδ: −0.057
9
Δδ: +0.031
H
5
4
6
4a
3
H
7
8a
2
O
8
1
Δδ: +0.041
MeO
Δδ: −0.004
H
O
Δδ: −0.034